Polymer 49 (2008) 3301–3309

Contents lists available at ScienceDirect

Polymer

journal homepage: www.elsevier.com/locate/polymer

Effects of organoclay platelets on morphology and mechanical properties in PTT/EPDM-*g*-MA/organoclay ternary nanocomposites

Kunyan Wang, Yanmo Chen*, Yu Zhang

State Key Laboratory for Modification of Chemical Fibers and Polymer Materials, College of Material Science and Engineering, Donghua University, Shanghai 201620, PR China

ARTICLE INFO

Article history:
Received 25 March 2008
Received in revised form 8 May 2008
Accepted 10 May 2008
Available online 22 May 2008

Keywords:
PTT/EPDM-*g*-MA blend
Morphology
Mechanical properties

ABSTRACT

The addition of up to 6 part per hundred (phr) of an organoclay to a 80/20 (w/w) PTT/EPDM-*g*-MA blend led to ternary compounds that came together as a means of balancing stiffness/strength versus toughness/ductility. The effect of organoclay platelets on morphologies and mechanical properties of PTT/EPDM-*g*-MA/organoclay ternary nanocomposites had been studied by SEM, TEM, WAXD, and mechanical testing. For the 80/20 (w/w) blend, the clay platelets are located inside the dispersed domains of EPDM-*g*-MA phase. The clay platelets do not act effectively as a barrier for the coalescence of the dispersed domains. The complex viscosities (η^*) of the 80/20 (w/w) PTT/EPDM-*g*-MA blend increased with the amount of the organoclay increasing, which are proposed as the reason for the dispersed domain size (D) that becomes smaller at higher clay content. Mechanical tests show that the Young's modulus increases, whereas the tensile strength and the impact strength decrease when the content of the clay increases.

1. Introduction

Fillers play important roles in modifying the desirable properties of polymers and reducing the cost of their composites. Among the inorganic materials used as additives or reinforcements to improve the properties of polymers, layered silicates, such as MMT, have recently received a great deal of attention [1–3]. Pristine-layered silicates usually contain hydrated Na^+ or K^+ and can interact only with hydrophilic polymers. To ensure interfacial interactions of the layered silicate with other hydrophobic polymer matrices, the hydrophilic-layered surface must be converted to an organophilic surface. Depending upon the interaction between the clay and the polymer, three different types of nanocomposites are known: phase separated, intercalated, and exfoliated structures. Several polymers, for instance, polyamide 6 (PA6) [4,5], poly(propylene) (PP) [6,7] epoxy [8,9] and polymer liquid crystal [10], have been employed.

Poly(trimethylene terephthalate) (PTT) belongs to the thermoplastic aromatic polyester family. PTT is now a potential competitor of PBT and PET in packing, textile, and engineering thermoplastic markets because its raw material, 1,3-propanediol, has a recent breakthrough in synthesis with reduced price. Due to some advanced properties such as enhanced tensile flexural strength, thermal and barrier properties, lots of studies on nanocomposites with PTT matrix have been carried out [11–13]. However, the incorporation of clay usually results in a deterioration of the strain-related end properties such as notched impact strength. Rubber addition is the usual technique to improve toughness in polymers. Ternary nanocomposites have attracted great attention in both academic and industry in order to achieve satisfied balanced properties [14–16]. Ahn et al. [17] studied the rubber toughening of nylon 6 nanocomposites. They found that the addition of clay affected the dispersion of the rubber phase resulting in larger and more elongated rubber particles. Khatua et al. [18] found that for the N6/ERP blend, the dispersed domain size (D) of EPR phase in the N6 matrix decreased significantly even if a small amount of the organoclay was added. As long as the clay becomes exfoliated in the matrix, the exfoliated clay plates effectively prevent the coalescence of the dispersed domains.

However, there is little research on toughened PTT-based nanocomposties. In this work, both EPDM-*g*-MA rubber and organoclay have been used to prepare the PTT/EPMD-*g*-MA/clay ternary nanocomposites. Our focus is to study the role of organoclay platelets on polymer blends of PTT/EPMD-*g*-MA.

2. Experimental section

2.1. Materials

PTT was purchased from the Shell Chemical Company (USA) and the trade name is CP509200 with $T_m = 225.6\ ^\circ C$. Intrinsic viscosity of the PTT chip is 0.935 dl/g and the number-average molecular weight is 38,000. Another PTT (PTT-L) with lower intrinsic viscosity (0.519 dl/g) was synthesized in our lab [19]. The number-average molecular weight is 28,000. Ethylene–propylene–diene copolymer

* Corresponding author. Tel.: +86 13761341277.
E-mail addresses: wky@mail.dhu.edu.cn (K. Wang), yanmochen@tom.com (Y. Chen).

0032-3861/$ – see front matter © 2008 Elsevier Ltd. All rights reserved.
doi:10.1016/j.polymer.2008.05.025

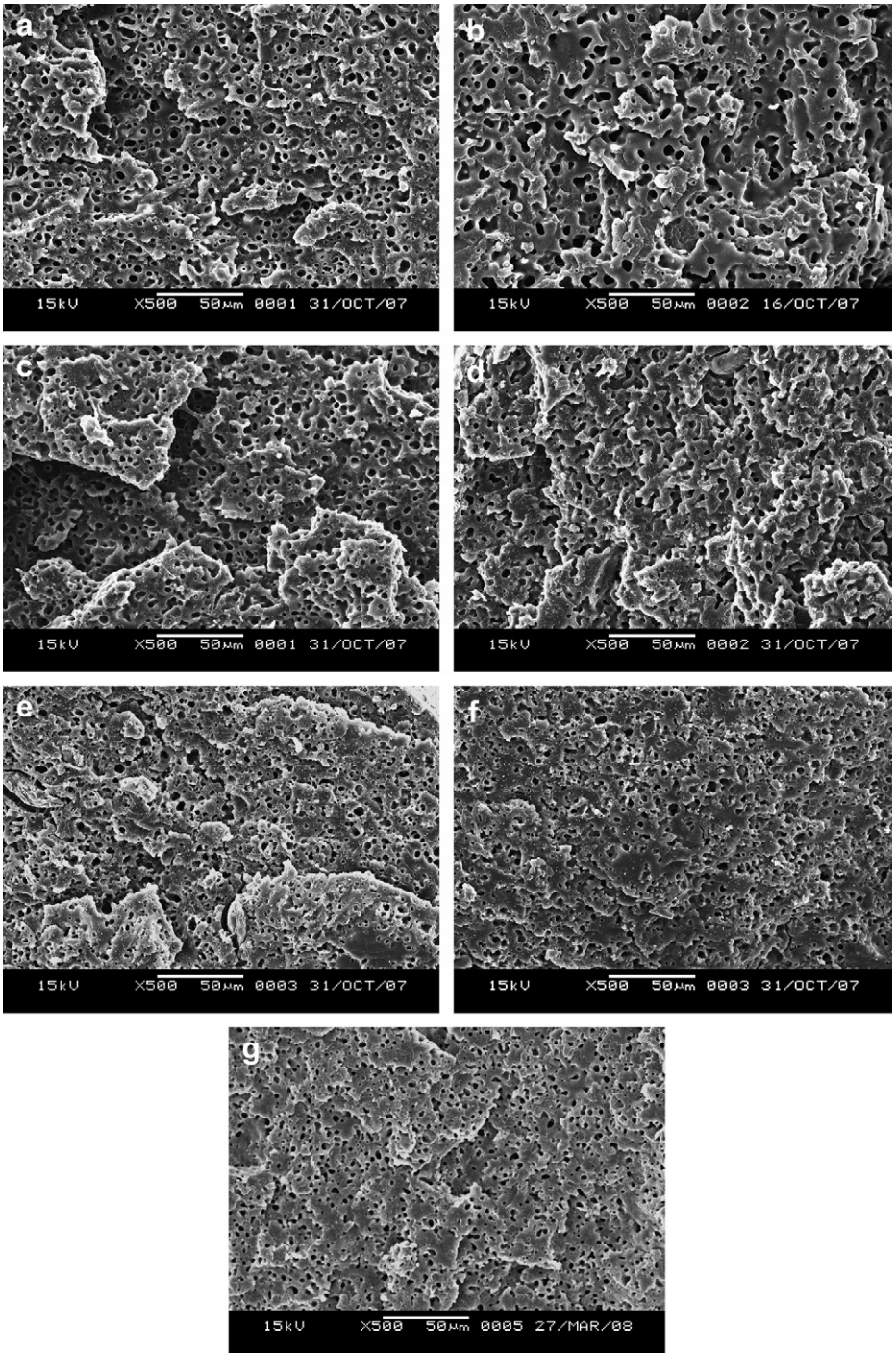

Fig. 1. SEM images of 80/20 (w/w) PTT/EPDM-*g*-MA blends with various amounts of the clay. The amount of the clay (in phr) is (a) 0; (b) 1; (c) 2; (d) 3; (e) 4; (f) 5 and (g) 6.

grafted with maleic anhydride (EPDM-*g*-MA) was provided by Shanghai Sunny New Technology development Co. Ltd; the grafted rate was 0.8%.

Organoclay (trade name is DK2) with particle size of less than 50 μm was supplied by Zhejiang FengHong Clay Co. Ltd. (China). Organo-modifier is methyl tallow bis(2-hydroxyethyl) ammonium and DK2 has the cation exchange capacity of 120 meq/100 g.

2.2. Specimens preparation

One blend composites 80/20 (W/W) PTT/EPDM-*g*-MA with various amounts of the organoclay (0–6 phr) were prepared by melt mixing in a Haake Rheocorder having a capacity of about 50 cm^3 at 235 °C and 120 rpm for 10 min. Before melt mixing, all polymers and the organoclay were completely dried in a vacuum oven at 80 °C for 12 h. The ternary polymer nanocomposites will be named by their OMMT content; i.e. PEC1 indicates an 80/20/1 PTT/EPDM-*g*-MA/organoclay blend, where P stands for PTT, E stands for EPDM-*g*-MA, and C stands for organoclay.

2.3. Characterizations

The *d* spacing of the layer structure of the organoclay itself as well as that in PTT/EPDM-*g*-MA nanocomposites was examined by

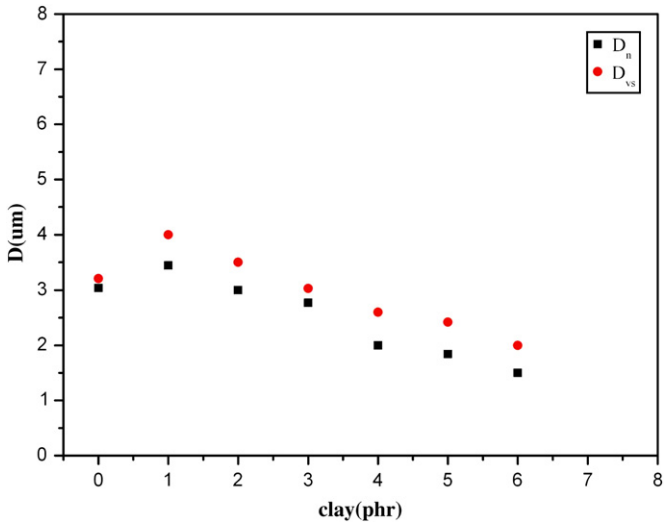

Fig. 2. Plot of D_n and D_{vs} of the 80/20 (w/w) PTT/EPDM-*g*-MA blend versus the amount of the clay.

using a wide-angle X-ray diffractometer (WAXD). Sample films (0.25–0.50 mm thickness) were prepared by compression molding the pellets in a Carver melt press. The length and width of all test samples are 20 mm and 15 mm, respectively. The wavelength of the monochromated X-ray from Cu Kα radiation is 0.154056 nm. The scanning angle 2θ range was 1–10° with a scanning rate of 2°/min.

The specimens were cryogenically fractured in liquid nitrogen, and then were etched in boiling toluene for 1 h to selectively dissolve the rubber particles. And the phase morphology was observed in a JSM-5600LV SEM instrument operating at an accelerating voltage of 5 kV after the surface was coated with gold powder. The number-average (D_n) and the volume-to-surface area average (D_{vs}) domain diameters were obtained with a MIVNT Microsoft. The cross-sectional area (A_i) of each particle in the SEM micrograph was measured and then converted into the diameter (D_i) of a circle having the same cross-sectional area by using the following relation.

$$D_i = 2(A_i/\pi)^{1/2}$$

Then, D_n and D_{vs} were obtained by

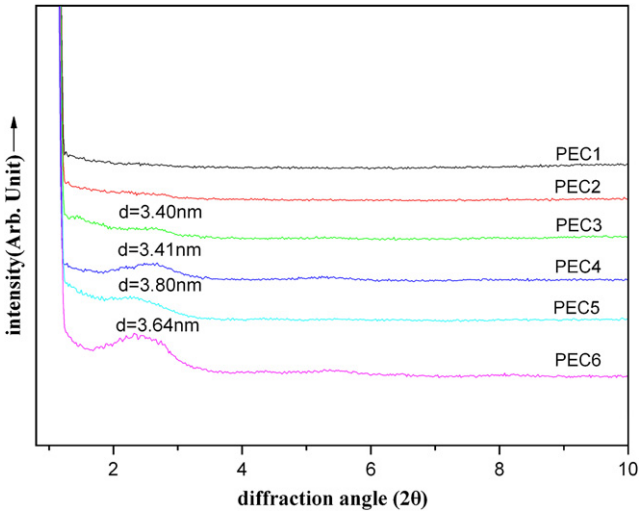

Fig. 3. WAXD patterns of the 80/20 (w/w) PTT/EPDM-*g*-MA blends with various amounts of the clay.

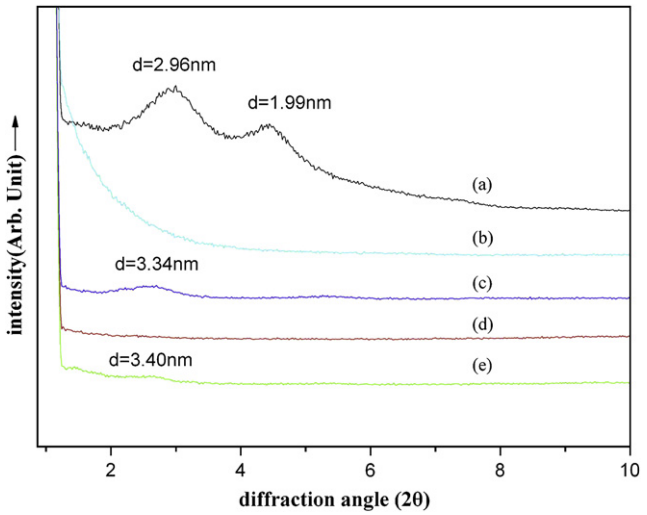

Fig. 4. WAXD profiles of the clay itself (a) and various nanocomposites; (b) EPDM/clay; (c) PTT/clay; (d) 80/20 (w/w) PTT/EPDM-*g*-MA/clay was etched out by toluene; (e) 80/20 (w/w) PTT/EPDM-*g*-MA/clay. All nanocomposites contained 3 phr of the clay.

$$D_n = \sum D_i/N$$

$$D_{vs} = \sum D_i^3/\sum D_i^2$$

where N is the total number of dispersed domains (200–300) observed in the SEM image.

The location of the clay in the blend was studied by transmission electron microscopy (TEM H-800) using an acceleration voltage of 100 kV. The samples were ultrathin-sectioned at 60–80 nm with a Reicher ultracut cryo microtome. On the other hand, EPDM-*g*-MA was also analyzed. To do so, ultramicrotomed samples were exposed to ruthenium tetroxide (RuO_4) and stained for 20 min.

An Advanced Rheometric Expansion System (ARES TA Instrument) was used to conduct for all samples with parallel plates of 25 mm diameter and about 1 mm thickness at 235 °C under a nitrogen environment. The frequency sweep was carried out within the frequency range of 0.1–100 rad/s at a strain of 0.5%, which is well within the linear viscoelastic range.

The tensile tests were performed in a universal testing machine according to ASTM D-638. The dog-bone-shaped specimens with gauge lengths of 7.62 mm were prepared by micro-injector made in USA; crosshead speed was set up at 10 mm/min. Young's modulus was calculated by linear regression of the stress data versus strain data from the initial strain to the data before the maximum strain. For each sample, the data reported are the average of five to seven specimens.

The impact experiment was carried out on an RESIL impact tester according to ASTM D-256. The notches (depth 2.54 mm and radius 0.25 mm) were machined after injection molding. A minimum of 10 impact specimens was tested for each reported value.

3. Results and discussion

3.1. Phase morphology

Fig. 1 shows the SEM images of 80/20 (W/W) PTT/EPDM-*g*-MA blends with various amounts of the organoclay. Interestingly, when a very small amount of organoclay (1 part per hundred (phr)) is used, the dispersed domain size (D) of EPDM-*g*-MA phase increases. As the amount of the organoclay increases, the D becomes smaller. On the basis of SEM images, the plot of D_n and D_{vs} versus

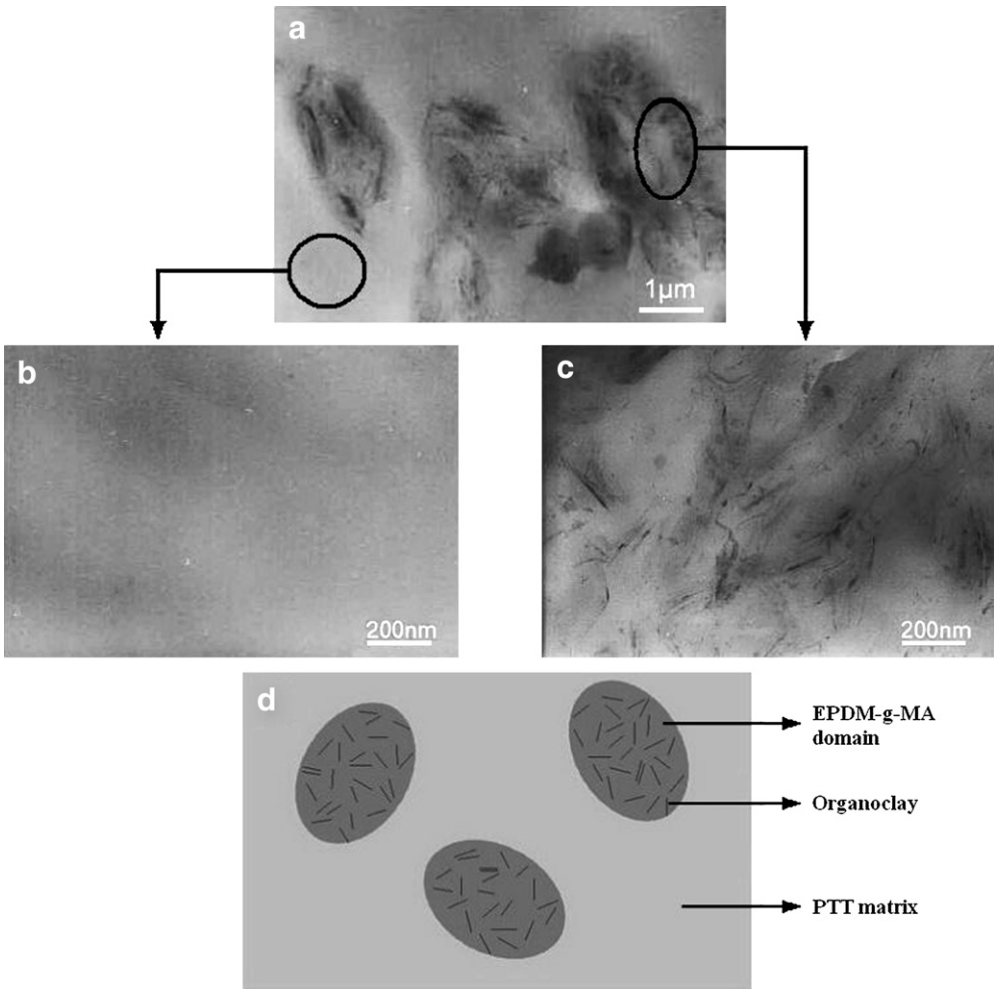

Fig. 5. TEM images of 80/20 (w/w) PTT/EPDM-*g*-MA blends with 3 phr of the clay: (a) lower magnification; (b) higher magnification of PTT domain; (c) higher magnification of EPDM-*g*-MA matrix; (d) schematic for the role of the clay platelets on the immiscible polymer blend. (The deep gray area represents the EPDM-*g*-MA phase. The gray area represents the PTT matrix and the black lines correspond to clay platelets).

the amount of the clay is shown in Fig. 2. It can be seen that an increase in D was found at lower amounts of the clay, and then a slow but gradual decrease in D was observed with further increasing the amount of the clay. This result is similar to that of the PA6/mSEBS nanocomposites [20].

3.2. Dispersed clay

Fig. 3 shows the WAXD patterns of PEC1–PEC6. In PEC1 and PEC2, the characteristic peak of the organoclay disappeared between 2° and 10°. The absence of the characteristic peak of the organoclay in PEC1 and PEC2 indicates that the clay platelets are completely exfoliated in either PTT or EPDM-*g*-MA. In PEC3–PEC6, the diffraction peaks shifted to lower angles corresponding to the d spacings of 3.40 nm, 3.41 nm, 3.80 nm, and 3.60 nm, respectively.

To investigate why D of the blend firstly increases with 1 phr clay, then D decreases with increasing amount of the clay, we first consider the clay dispersion in neat polymers as well as the blend. Fig. 4 shows the WAXD patterns of the clay itself and the nanocomposites with PTT, EPDM-*g*-MA, and 80/20 (W/W) PTT/EPDM-*g*-MA blend. The peak corresponding to the basal spacing of the organoclay appears at $2\theta = 2.98°$ (the corresponding d_{001} spacing is 2.96 nm). For PTT/organoclay nanocomposites, the characteristic peak of the clay shifted to lower angles corresponding to an increase in the d spacing to 3.34 nm, which suggests that PTT chains only intercalated the clay. This result is consistent with previous result [21,22]. The intercalation of PTT chains inside the clay particles disorders the layered structure of the clay and, thus, a decrease in WAXD coherent layered scattering is observed [23,24]. On the other hand, for EPDM-*g*-MA/organoclay nanocomposites, the characteristic peak of the clay did not appear even at smallest value of 2θ of 0.5°, which is the lower limit of the WAXD. This indicates that the clay platelets are completely exfoliated by the EPDM-*g*-MA chains. Finally, for the nanocomposite of 80/20 (w/w) PTT/EPDM-*g*-MA blends with 3 phr of the clay, a broad and very weak diffraction peak appears around $d_{001} = 3.40$ nm. The presence of this peak represents the small part of clay that does not completely exfoliate during the processing. More interestingly, when the EPDM-*g*-MA disperse phase in the 80/20 (W/W) PTT/EPDM-*g*-MA blend with 3 phr of clay was completely etched out by toluene, WAXD patterns of the clay did not appear. We also observed the same result for the 80/20 (W/W) PTT/EPDM-*g*-MA blend with other contents of clay. They show the similar behavior and are not shown in Fig. 4.

The TEM image of the 80/20 (W/W) PTT/EPDM-*g*-MA blend with 3 phr of the clay is given in Fig. 5. The deep gray dispersed domains correspond to the EPDM-*g*-MA phases. The gray domains correspond to the PTT matrix and the black lines correspond to the clay platelets. Since we could not see any discernible clay platelets in PTT domains, as shown in Fig. 5b, we consider that almost all the clay platelets exist in EPDM-*g*-MA with exfoliation and small amount of intercalation (Fig. 5c), although it cannot be excluded that a minor amount of clay was incorporated in PTT matrix. The

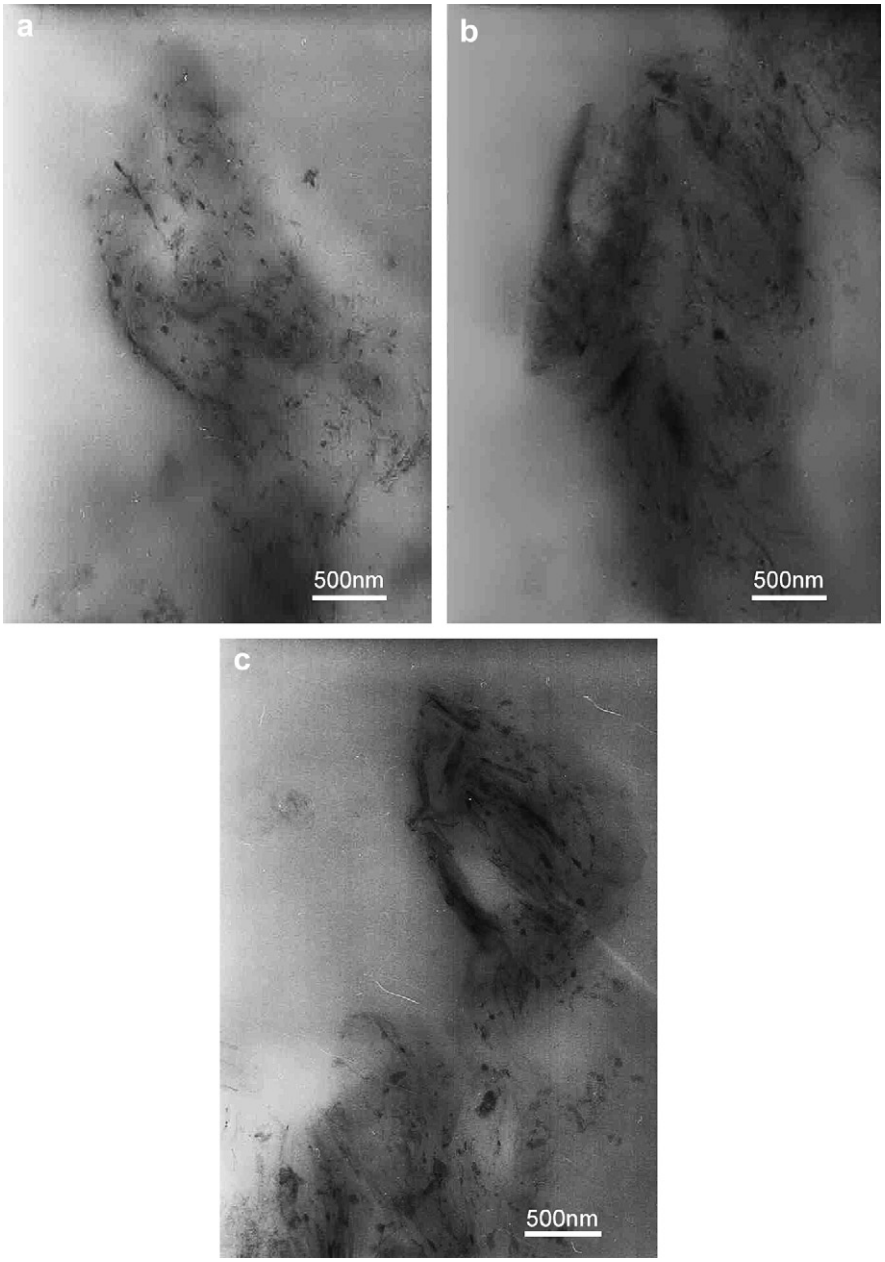

Fig. 6. TEM images of 80/20 (w/w) PTT/EPDM-*g*-MA blends with (a) 2 phr; (b) 4 phr and (c) 6 phr of the clay.

preference of the clay existing in which domain is due to the difference of polarity between organoclay with polymer chains [25,26]. The group of maleic anhydride (MA) of EPDM is more polar than PTT chain, although EPDM is non-polar polymer, thus, the clay might be easily exfoliated by EPDM-*g*-MA chains compared with PTT chains. On the basis of these results, we drew a schematic of the role of clay on PTT/EPDM-*g*-MA blend in Fig. 5d.

Furthermore, in order to know whether other samples have the same morphology, the TEM image of the 80/20 (w/w) PTT/EPDM-*g*-MA blends with 2 phr, 4 phr and 6 phr of the clay, is given in Fig. 6. The rubber particles have a more extended ellipsoidal shape. It is also observed that the clay platelets penetrate and intrude into the EPDM-*g*-MA rubber particles. This might be explain that why the EPDM-*g*-MA disperse phase in the 80/20 (W/W) PTT/EPDM-*g*-MA blend with various amounts of clay was completely etched out by toluene, WAXD patterns of the clay did not appear. Almost all the clay platelets exist in the EPDM-*g*-MA with exfoliation or intercalation; thus they must also be etched out by toluene with the EPDM-*g*-MA. So the WAXD patterns of the clay disappear. The TEM images of samples with 1 phr and 5 phr contents of clay showed similar morphology and are not shown.

In the organoclays some excess surfactant is usually present [27] which probably dissolves in the matrix during processing. This surfactant may interact with the maleic anhydride substitution of the rubber, thus decreasing the compatibilizing efficiency of the maleic substitution leading to a large rubber particle size. This is in agreement with Gonzalez's report by researched PA6/mSEBS/clay nanocomposites. To test the effects of the surfactant, pure surfactant was added to 2 phr and 3 phr clay of 80/20 (w/w) PTT/EPDM-*g*-MA blend. The dispersed domain size (D) of EPDM-*g*-MA phase is almost similar to the D of blend without excess surfactant. We found that the addition of surfactant did not lead to an increase in particle size. Recently, Khatua et al. [18] found that as long as the clay becomes exfoliated in the matrix, the exfoliated clay platelets effectively prevent the coalescence of the dispersed domains, whereas the exfoliated platelets located inside the dispersed

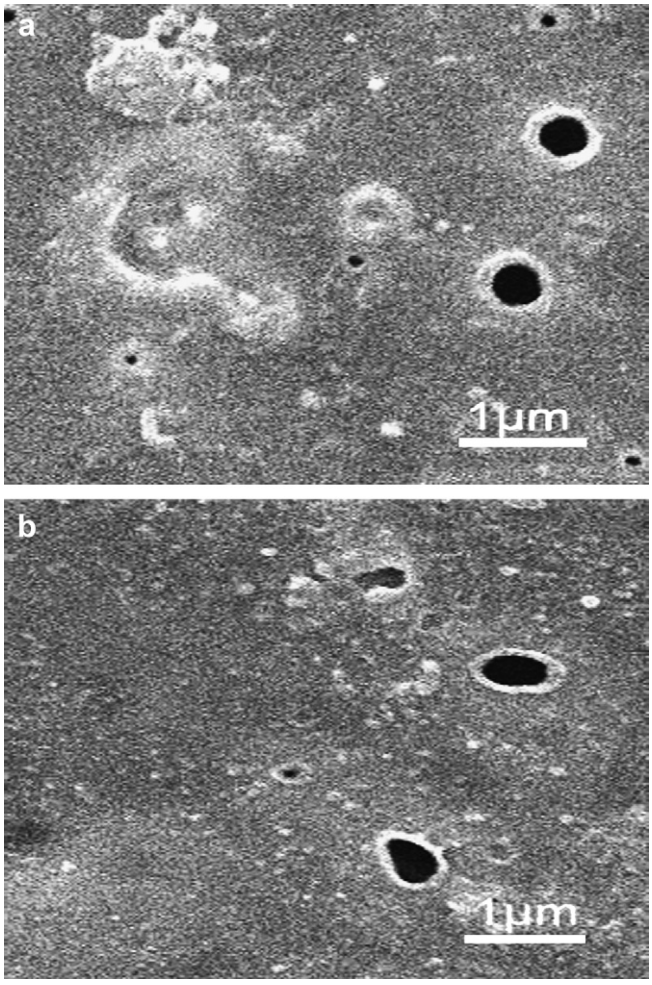

Fig. 7. SEM images of 99/1 (w/w) PTT/EPDM-*g*-MA blends with (a) 5 phr and (b) 6 phr of the clay.

domains do not act effectively as a barrier for the coalescence of the dispersed domains. This may be the reason for the phenomenon above that when a very small amount of organoclay (1 phr) is used, the dispersed domain size (D) of EPDM-*g*-MA phase increases.

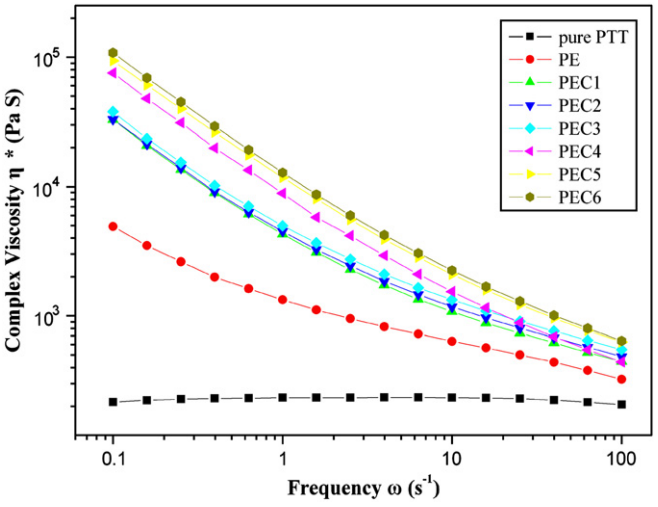

Fig. 8. Plot of complex viscosity (η^*) with frequency (ω) at 235 °C for pure PTT, PE and PEC1–PEC6.

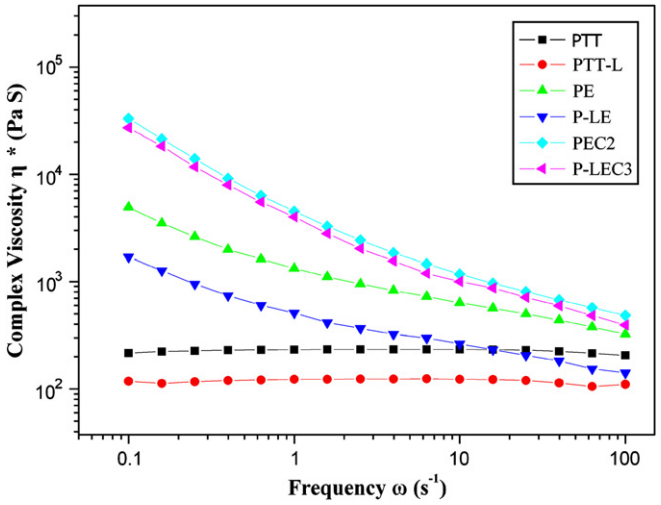

Fig. 9. Plot of complex viscosity (η^*) with frequency (ω) at 235 °C.

To study the barrier effect of organoclay on the PTT/EPDM-*g*-MA blends, we also studied the morphology of 99/1 (w/w) PTT/EPDM-*g*-MA blends with 5 phr and 6 phr of the clay. We chose 99/1(w/w) PTT/EPDM-*g*-MA blends in order to reduce the error of the dispersed domain size (D) of EPDM-*g*-MA phase calculated by MIVNT Microsoft. The blends with 5 phr and 6 phr of the clay were decided to use due to the observation that the two nanocomposites have almost the same viscosity. Thus they could eliminate the effect of the viscosity. Fig. 7 shows SEM image of these blends. It is seen in Fig. 7 that D_n for 99/1 (w/w) PTT/EPDM-*g*-MA blends with 5 phr of the clay was 0.60 μm. D_n of the 99/1 (w/w) PTT/EPDM-*g*-MA blends with 6 phr of the clay was 0.58 μm, which is almost the same as that with 5 phr of the clay. This might clearly indicate that the clay did not play a role of a barrier for the coalescence of the dispersed domains.

3.3. Melt rheological behavior

We consider that the decreased domain size in the 80/20 (w/w) blend by the addition of the clay (more than 1 phr) might be attributed to the increased viscosity by the clay. To check this possibility, we measured the complex viscosities (η^*) of pure PTT and 80/20 (w/w) PTT/EPDM-*g*-MA blend without and with the clay, as shown in Fig. 8. It was seen that η^* increased with the amount of

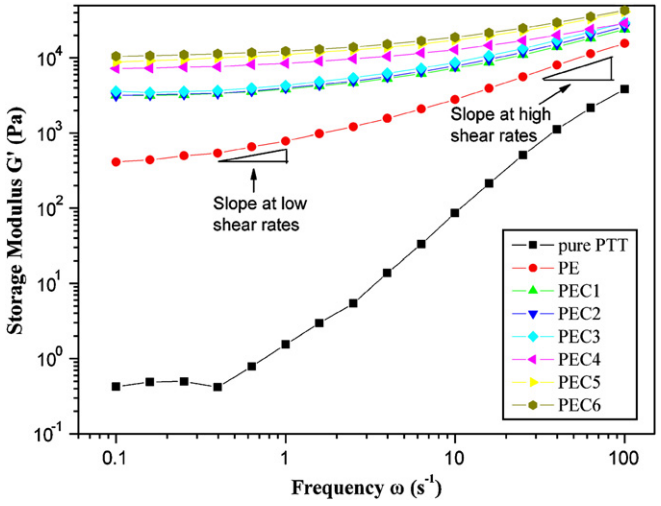

Fig. 10. Variation of the storage modulus (G') as a function of frequency for the 80/20 (w/w) PTT/EPDM-*g*-MA blend with various amounts of the clay.

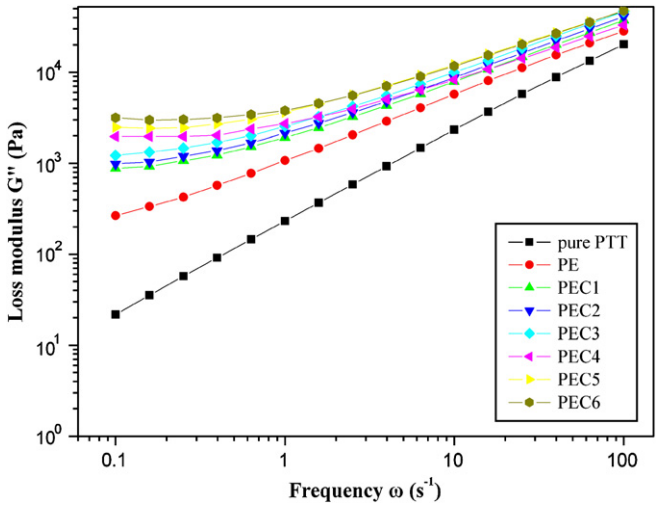

Fig. 11. Variation of the loss modulus (G'') as a function of frequency for the 80/20 (w/w) PTT/EPDM-*g*-MA blend with various amounts of the clay.

the organoclay increasing. The effect of the clay amount on the complex viscosity was quite prominent at low frequency, and decreased with increasing frequency because of the shear thinning function. Thus, the decrease in D of dispersed EPDM-*g*-MA domains in the 80/20 (w/w) PTT/EPDM-*g*-MA/clay (more than 1 phr) nanocomposite may be due to increased viscosity of matrix phase (PTT). This was also observed in PP [28–30], and low molecular weight PA6 [31] with clay.

In order to clarify the effect of matrix viscosity on morphology of the 80/20 (w/w) PTT/EPDM-*g*-MA blend, we also studied the blend morphology with another PTT (PTT-L) with 44% lower viscosity than that of PTT, as shown in Fig. 9. It is seen that the viscosity of the 80/20 (w/w) PTT-L/EPDM-*g*-MA blend with 3 phr of the clay is almost the same as that of the 80/20 (w/w) PTT/EPDM-*g*-MA blend with 2 phr of the clay. We observed that the D_n of the 80/20 (w/w) PTT-L/EPDM-*g*-MA blend was 4.55 μm, which is greater than that of the 80/20 (w/w) PTT/EPDM-*g*-MA blend (3.04 μm). Moreover, as shown previously, the D_n of the 80/20 (w/w) PTT/EPDM-*g*-MA blend with 2 phr of the clay was 3.00 μm, almost the same as that of the 80/20 (w/w) PTT-L/EPDM-*g*-MA blend with 3 phr of the clay (3.07 μm). From these results, we concluded that the main effect of the decrease in D in the 80/20 (w/w) PTT/EPDM-*g*-MA blend in the presence of the clay is due to the increased viscosity of the matrix polymer but not due to effect of the clay as a barrier for the coalescence of the dispersed domains.

A deeper insight into the morphology-dependent flow behavior was expected from the rheological measurements performed in the viscoelastic range. Figs. 10 and 11 show the plots of the storage (G') and loss (G'') moduli versus different frequencies for all samples,

Table 1
Storage modulus (G') values and their slopes as a function of frequency in double logarithmic scale at low (1 rad/s) and high frequencies (100 rad/s)

	Storage modulus (G')			
	Low frequency (at 1 rad/s)		High frequency (at 100 rad/s)	
	Value (Pa)	Slope	Value (Pa)	Slope
PTT	1.55	1.37	3828.09	1.33
PE	784.43	0.46	15,650.30	0.72
PEC1	3838.24	0.32	24,133.10	0.57
PEC2	3964.79	0.30	26,120.10	0.55
PEC3	4294.45	0.26	29,397.70	0.53
PEC4	8477.42	0.16	29,409.40	0.38
PEC5	11147.70	0.15	41,169.60	0.35
PEC6	12337.40	0.13	43,139.20	0.32

Table 2
Loss modulus (G') values and their slopes as a function of frequency in double logarithmic scale at low (1 rad/s) and high frequencies (100 rad/s)

	Loss modulus G'			
	Low frequency (at 1 rad/s)		High frequency (at 100 rad/s)	
	Value (Pa)	Slope	Value (Pa)	Slope
PTT	233.11	1.00	20,228.40	0.89
PE	1073.76	0.70	28,341.60	0.82
PEC1	1916.07	0.65	33,116.80	0.80
PEC2	2144.84	0.57	37,213.20	0.70
PEC3	2538.10	0.56	40,894.40	0.68
PEC4	2718.24	0.55	46,333.40	0.67
PEC5	3628.51	0.42	47,393.40	0.63
PEC6	3729.64	0.41	47,424.20	0.62

respectively. Both G' and G'' increased monotonically in the covered frequency range when organoclay was introduced to the 80/20 (w/w) PTT/EPDM-*g*-MA blend. The increase in the modulus is prominent in the lower frequency range. This is due to the fact that at low frequencies there is enough time to unravel the entanglements so that a large amount of relaxation occurs, which results in lower loss and storage moduli. However, when a polymer sample is deformed at a large frequency, the entanglements do not have the time to relax and, therefore, the modulus increases. It was also found that a noticeable qualitative change in the moduli versus frequency plots was observed as the clay content was increased from 3 to 4 phr.

According to Li et al. [32], changes of G' and G'' in the viscoelastic range sensitively reflect the effect of clay dispersion. The higher the slope, the less stable the clay dispersion is. Tables 1 and 2 list the slope value of both G' and G'' in the low frequency range. More exactly, the slope value was read at both 1 rad/s and 100 rad/s values. The slope determination is shown in Fig. 10. At lower frequency (at 1 rad/s) the polymer chains are fully relaxed and thus alterations in G' and G'' including slopes are likely to be linked to the effect of the clay dispersion. It is shown from Tables 1 and 2 that the slope in the low frequency viscoelastic range decreases with organoclay loading. This holds for all samples at 1 rad/s and 100 rad/s frequencies. This slope change indicates that the nanocomposites attained a pseudo solid-like behavior due to the nanoreinforcing effect of the intercalated/exfoliated clay. Similar results were reported by Hoffmann et al. [33]. The higher the G' moduli and the smaller the slope is (at low frequency), the more pronounced the interaction between the clay platelets and their tendency to form a three-dimensional superstructure [33]. Therefore, when more clay is added to 80/20 (w/w) PTT/EPDM-*g*-MA, the clay

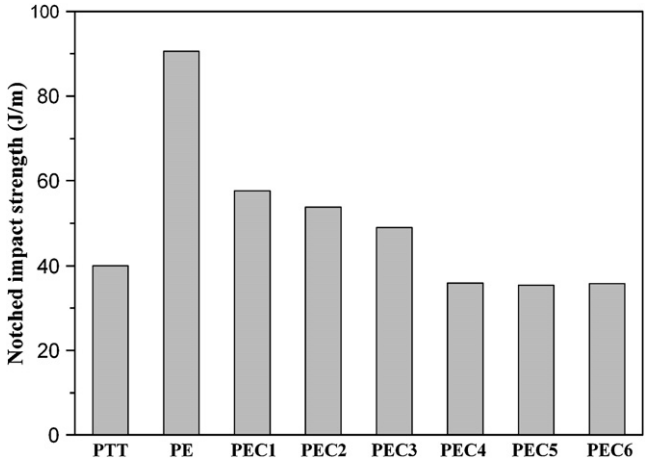

Fig. 12. The notched Izod impact strength versus the clay content in the 80/20 (w/w) PTT/EPDM-*g*-MA blends.

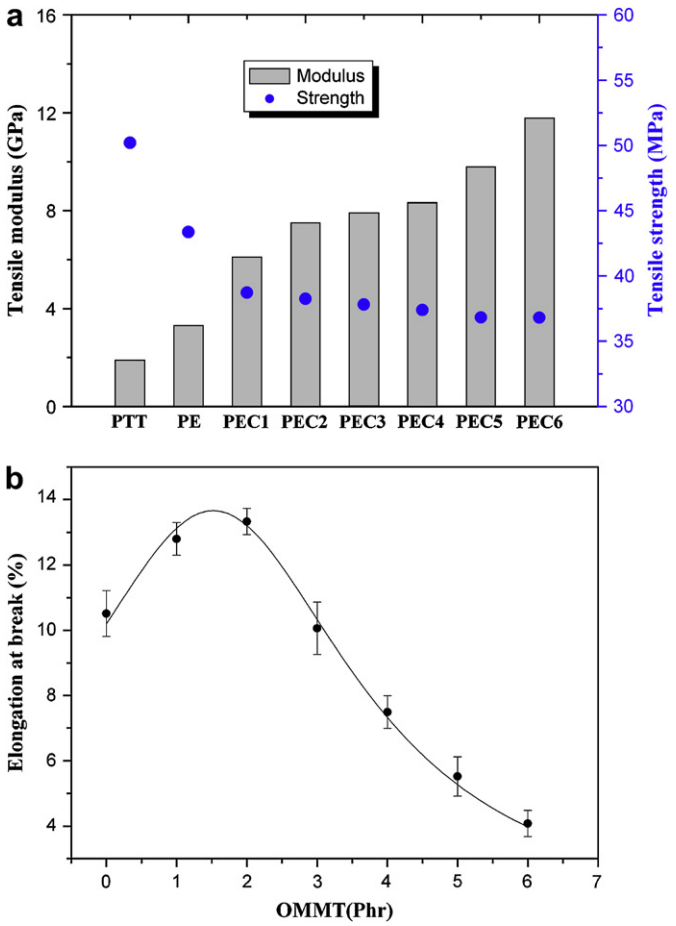

Fig. 13. (a) Young's modulus and tensile strength; (b) elongation at break of 80/20 (w/w) PTT/EPDM-*g*-MA blends at different clay contents.

platelets tend to form a three-dimensional superstructure in the dispersion phase of EPDM-*g*-MA domains.

3.4. Mechanical properties

The impact strength for a material describes the energy required to break the specimen. The magnitude of impact strength reflects the ability of material to resist impact. Notch Izod impact strength emphasizes the energy to propagate a crack under impact load. Impact strength of the clay reinforced polymeric composites is complex because of the role of the clay and the clay/matrix interface in addition to the polymer. The notched impact strength versus the clay content in the 80/20 (w/w) PTT/EPDM-*g*-MA blend is shown in Fig. 12. The impact strength of PTT is also shown as a reference. We found that the impact strength of the 80/20 (w/w) PTT/EPDM-*g*-MA blend without clay improved more than two times compared to the pure PTT, which clearly indicates that EPDM-*g*-MA rubber acts as a toughener for PTT. The impact strength of the 80/20 (w/w) PTT/EPDM-*g*-MA with 1 phr of the clay was 57.62 J/m, which increased about 25% of the pure PTT. When adding to 3 phr clay, the impact strength slightly decreased, indicating that clay have a positive contribution to impact strength of PTT/EPDM-*g*-MA blend. The impact strength then remained constant up to 6 phr clay content, which was slightly smaller than that of the pure PTT.

Fig. 13 plots the Young's modulus, tensile strength, and elongation at break at different clay contents. As can be seen, the Young's modulus continuously increased with the clay content. These modulus increases are very similar to those observed in the rubber toughening of PA6 [34] and PP [35] nanocomposites, which indicate that clay can improve the stiffness of the materials. However, as more clays are added to the blends, the tensile strength decreases (Fig. 13(a)) and the material becomes tough at clay contents below 3 phr, which can be seen from the increasing elongation at low clay content (Fig. 13(b)) The tensile strength is lower at high content of clay presumably because the adhesion between the clay and the polymer is weak [36]. Improved adhesion may be achieved by functionalizing the clay and/or polymer to create a better bond between the two materials. This will be the subject of another study.

4. Conclusion

In this study, we have shown that an organoclay plays an important role in the dispersed domain sizes in the blends of PTT/EPDM-*g*-MA. According to WAXD and TEM images, we concluded that almost all of exfoliated or intercalation clay platelets existed in the dispersed domains of EPDM-*g*-MA phase, resulting in the dispersed domain size (D) of EPDM-*g*-MA phase increase, when a very small amount of organoclay (1 part per hundred (phr)) is used. The main effect of the decrease in D in the 80/20 (w/w) PTT/EPDM-*g*-MA blend in the presence of the more clay is due to the increased viscosity of the matrix polymer but not due to effect of the clay as a barrier for the coalescence of the dispersed domains. When more clay is added to 80/20 (w/w) PTT/EPDM-*g*-MA, the clay plateles tend to form a three-dimensional superstructure in the dispersion phase of EPDM-*g*-MA domains. The mechanical properties of the ternary nanocomposites are improved compared to the pure PTT, but the improvement is relatively small. The Young's modulus increases with content of the clay.

References

[1] Hasmukh AP, Rajesh S, Hari CB, Raksh VJ. Preparation and characterization of phosphonium montmorillonite with enhanced thermal stability. Appl Clay Sci 2007;35:144–200.
[2] Wang Y, Zhang Q, Fu Q. Compatibilization of immiscible poly(propylene)/polystyrene blends using clay. Macromol Rapid Commun 2003;24(3):231–5.
[3] Li YJ, Shimizu H. Co-continuous polyamide 6 (PA6)/acrylonitrile–butadiene–styrene (ABS) nanocomposites. Macromol Rapid Commun 2005;26(9):710–5.
[4] Kim SW, Jo WH, Lee MS, Ko MB, Jho JY. Effects of shear on melt exfoliation of clay in preparation of nylon 6/organoclay nanocomposites. Polym J 2002;34(3):103–11.
[5] Fornes TD, Hunter DL, Paul DR. Nylon-6 nanocomposites from alkylammonium-modified clay: the role of alkyl tails on exfoliation. Macromolecules 2004;37(5):1793–8.
[6] Gianelli W, Ferrara G, Camino G, Pellegatti G, Rosenthal J, Trombini RC. Effect of matrix features on polypropylene layered silicate nanocomposites. Polymer 2005;46(18):7037–46.
[7] Wang Y, Chen FB, Wu KC. Effect of the molecular weight of maleated polypropylenes on the melt compounding of polypropylene/organoclay nanocomposites. J Appl Polym Sci 2005;97(4):1667–80.
[8] Frohlich J, Thomann R, Mulhaupt R. Toughened epoxy hybrid nanocomposites containing both an organophilic layered silicate filler and a compatibilized liquid rubber. Macromolecules 2003;36(19):7205–11.
[9] Chen B, Liu J, Chen HB, Wu JS. Synthesis of disordered and highly exfoliated epoxy/clay nancomposites using organoclay with catalytic function via acetone–clay slurry method. Chem Mater 2004;16:4864–6.
[10] Zhang BQ, Ding YU, Chen P, Liu CY, Zhang J, He JS, et al. Fibrillation of thermotropic liquid crystalline polymer enhanced by nano-clay in nylon-6 matrix. Polymer 2005;46(14):5385–95.
[11] Dangayach K, Chuah H, Gergen W, Dalton P, Smith F. Poly(trimethylene terephthalate) (PTT) – new opportunity in engineering thermoplastic applications. Annu Tech Conf Soc Plast Eng 1997;55(2):2097–101.
[12] Chang JH, Mun MK, Kim JC. Poly(trimethylene terephthalate) nanocomposite fibers comprising different organoclays: thermomechanical properties and morphology. J Appl Polym Sci 2006;102:4535–45.
[13] Chang JH, Kim SJ, Im S. Poly(trimethylene terephthalate) nanocomposite fibers by in situ intercalation polymerization: thermo-mechanical properties and morphology. Polymer 2004;45:5171–81.
[14] Hong JS, Kung HN, Ahn KH, Lee SJ, Kim CY. The role of organically modified layered silicate in the breakup and coalescence of droplets in PBT/PE blends. Polymer 2006;47:3967–75.
[15] Yoo Y, Park CY, Lee SG, Choi KY, Kim DS, Lee JH. Influence of addition of organoclays on morphologies in nylon 6/LLDPE blends. Macromol Chem Phys 2005;206:878–84.

[16] Ray SS, Pouliot S, Bousmina M, Utracki LA. Role of organically modified layered silicate as an active interfacial modifier in immiscible polystyrene/polypropylene blends. Polymer 2004;45(25):8403–13.
[17] Ahn YC, Paul DR. Rubber toughening of nylon 6 nanocomposites. Polymer 2006;47:2830–8.
[18] Khatua BB, Dong JL, Hwang YK, Jin KK. Effect of organoclay platelets on morphology of nylon-6 and poly(ethylene-*ran*-propylene) rubber blends. Macromolecules 2004;37:2454–9.
[19] Chen XD, Hou G, Chen YJ, Yang K, Dong Y, Zhou H. Effect of molecular weight on crystallization, melting behavior and morphology of poly(trimethylene terephalate). Polym Test 2007;26:144–53.
[20] Gonzalez I, Eguiazabal JI, Nazabal J. Nanocomposites based on a polyamide 6/maleated styrene–butylene-*co*-ethylene–styrene blend: effects of clay loading on morphology and mechanical properties. Eur Polym J 2006;42:2905–13.
[21] Mishra JK, Chang YW, Choi NS. Preparation and characterization of rubber-toughened poly(trimethylene terephthalate)/organoclay nanocomposite. Polym Eng Sci 2007:863–70.
[22] Liu ZJ, Chen KQ, Yan DY. Crystallization, morphology, and dynamic mechanical properties of poly(trimethylene terephthalate)/clay nanocomposites. Eur Polym J 2003;39:2359–66.
[23] Kalgaonkar Rajendra A, Jog JP. Copolymer/layered silicate nanocomposites: the effect of the molecular size and molecular structure of the intercalant on the structure and viscoelastic properties of the nanocomposites. J Polym Sci Part B Polym Phys 2003;41:3102–13.
[24] Vaia RA, Giannelis EP. Polymer melt intercalation in organically-modified layered silicates: model predictions and experiment. Macromolecules 1997;30:8000–9.
[25] Alexandre M, Dubois P. Polymer-layered silicate nanocomposites: preparation, properties and uses of a new class of materials. Mater Sci Eng 2000;28:1–63.
[26] Giannelis EP, Krishnamoorti R, Manias E. Polymer–silicate nanocomposites: model systems for confined polymers and polymer brushes. Adv Polym Sci 1999;138:107–47.
[27] Morgan AB, Harris JD. Effects of organoclay Soxhlet extraction on mechanical properties, flammability properties and organoclay dispersion of polypropylene nanocomposites. Polymer 2003;44(8):2313–20.
[28] Galgali G, Ramesh C, Lele A. A rheological study on the kinetics of hybrid formation in polypropylene nanocomposites. Macromolecules 2001;34(4):852–8.
[29] Solomon MJ, Almusallam AS, Seefeldt KF, Somwangthanaroj A, Varadan P. Rheology of polypropylene/clay hybrid materials. Macromolecules 2001;34(6):1864–72.
[30] Gu SY, Ren J, Wang QF. Rheology of poly(propylene)/clay nanocomposites. J Appl Polym Sci 2004;91(4):2427–34.
[31] Fornes TD, Yoon PJ, Keskkula H, Paul DR. Nylon 6 nanocomposites: the effect of matrix molecular weight. Polymer 2001;42(25):9929–40.
[32] Li J, Zhou G, Wang G, Yu W, Tao Y, Liu Q. Preparation and linear rheological behavior of polypropylene–montmorillonite nanocomposites. Polym Compos 2003;24:323–31.
[33] Hoffmann KJ, Stoppelmann FC, Kim GM. Rheology of nanocomposites based on layered silicates and polyamide 12. Colloid Polym Sci 2000;278:629–36.
[34] Gonzalez I, Eguiazabal JI, Nazabal J. Compatibilization level effects on the structure and mechanical properties of rubber-modified polyamide-6/clay nanocomposites. J Polym Sci Part B Polym Phys 2005;43(24):3611–20.
[35] Modesti M, Lorenzetti A, Bon D, Besco S. Effect of processing conditons on morphology and mechanical properties of compatibilized polypropylene nanocomposites. Polymer 2005;46(23):10237–45.
[36] Lin B, Gelves GA, Haber JA, Sundararaj U. Electrical, rheological, and mechanical properties of polystyrene/copper nanowire nanocomposites. Ind Eng Chem Res 2007;46:2481–7.